Study of the electric arc dynamics in a cascaded-anode plasma torch

Céline Ruelle, Simon Goutier, Vincent Rat, Alan Keromnes, Christophe Chazelas, Érick Meillot

Study of the electric arc dynamics in a cascaded-anode plasma torch

Study of the electric arc dynamics in a cascaded-anode plasma torch

Céline RUELLE[a], Simon GOUTIER[a], Vincent RAT[a], Alan KEROMNES[a], Christophe CHAZELAS[a], Érick MEILLOT[b]

[a]IRCER, CNRS UMR 7315, University of Limoges, F-87068 Limoges, France

[b]CEA, DAM, Le Ripault, F-37260 Monts, France

Corresponding author: celine.ruelle@unilim.fr ; +33 (0)5 87 50 24 13

Abstract:

In plasma spraying process, the plasma jet stability depends on the electric arc movement inside the plasma torch. For conventional plasma torches with rod cathode and a large anodic surface, arc roots are free to move along the anode wall, leading to high plasma jet fluctuations. To overcome these instabilities, cascaded-anode plasma torches have been developed, reducing considerably the electric arc movement and thus the plasma jet fluctuations. Unfortunately, a small number of studies reports on the behaviour of theses torches including the arc instabilities and on electrode erosion process as well. In this work, several diagnostics have been set up to further understand the cascaded-anode plasma torch behaviour under different sets of operating conditions. Influence of plasma forming gas composition on the electric arc dynamic has been studied through anodic imaging. The issue of the intense plasma radiation masking is discussed since the light emitted by the arc column interferes with anodic arc roots observations. Multiple constricted arc roots have been observed and a preferential site for anodic arc root has been identified for all experimental conditions. The addition of a secondary plasma forming gas promotes a higher number of reattachments. The influence of the electric arc movement on plasma jet stability is also studied by following the plasma jet brightness fluctuations. The low

voltage fluctuation frequency is also observed on brightness spectra, which means that these fluctuations could have an impact on in-flight particle treatment

Keywords: cascaded-anode plasma torch, end-on imaging, anodic arc roots observation, masking issue, arc voltage fluctuations, thermal balances.

1. Introduction

Arc plasma torch is a device converting electric energy into thermal and kinetic energies. A high current arc is generated between two electrodes and dissipates its energy in plasma forming gases, creating a plasma jet characterized by a high temperature (> 10 000 K) and a high velocity (> 1 000 $m.s^{-1}$) [1]. This high energy medium can be used to melt and spray particles towards a substrate to form a coating by plasma spraying. The as-sprayed coatings are widely used in various industrial applications such as aeronautical and automotive fields, for instance [2]. Coatings properties depend on substrate parameters (nature, surface roughness, temperature) and on in-flight particle characteristics (velocity, temperature, melting state) [3, 4]. Particle treatment is influenced by plasma jet fluctuations which result from the electric arc movement. Electric arc can be divided in two zones: the arc column, delimited by an isotherm shell (T > 7 000 – 8 000 K) in which the gas electrical conductivity is significant to ensure the current transport [5], and the arc attachment that connects the arc column to the anode wall. Note that the arc column is expanded from the cathode tip where the cathodic jet is stabilized by means of plasma forming gases. Anodic arc root movement is exposed to two main forces, namely the drag force exerted by the gas flowing towards the nozzle exit, and the Lorentz force due to interaction between arc current and induced magnetic field [6]. These forces coupled to large scale arc shunting processes result in voltage fluctuations and therefore in electrical power variation.

For conventional plasma torches, characterized by a large anodic surface (Fig. 1 A), electric arc is free to move along the anode, leading to high voltage fluctuations (more than 70 % of the mean voltage) [7]. Several modes of instabilities have been identified, including steady, take-over, restrike or Helmholtz modes. The first one corresponds to a nearly stable behaviour of the arc due to a fixed location of the arc root leading to constant arc voltage. The take-over mode is characterized by a quasi-sinusoidal arc voltage signal obtained by a back and forth movement of the arc attachment. When plasma torch is operating under restrike mode, arc voltage signal

has a saw-tooth shape and large amplitude of voltage fluctuations occur due to a sudden upstream reattachment [8–11]. The Helmholtz mode is driven by pressure effects generated by torch design [12, 13]. It has to be underlined that a torch usually operates in a combination of the preceding modes. Bisson *et al*. [14] highlighted the influence of these voltage fluctuations on the characteristics of in-flight particles sprayed with a conventional plasma torch operating under restrike mode. The authors synchronized particles temperature and velocity measurements with voltage signal measurements and showed that the periodic arc voltage fluctuation (about 220 µs) is also observed on particles temperature and velocity signals. Goutier *et al*. [15] drew similar conclusions for certain operating conditions with an F4 plasma torch, depending on the arc voltage signal quality. As coatings properties depend on the state of in-flight particles, it means that voltage fluctuations, due to electric arc movement, directly influence the coating characteristics (porosity and number of unmelted particles) as shown in [16].

To overcome these instabilities, an alternative design of torch has been developed, named cascaded-anode plasma torch [17], schematized in Fig. 1 B. It comprises an additional stage called « neutrode stacking » allowing the extension of the arc length, and a reduced anodic surface. In such a design, the arc column length is much longer than that of the arc attachment region so that the mean voltage can be assigned to arc column and voltage fluctuations to anodic arc root movement.

Seshadri *et al*. [18] compared the characteristics of a conventional and a cascaded-anode plasma torch for a same plasma forming gas composition and drew the following conclusions : with a cascaded-anode plasma torch, mean voltages are higher and voltage fluctuations are reduced, an increasing current-voltage characteristic is obtained and the plasma jet is much more uniform in terms of temperature and velocity. However, one important challenge with such a torch design is to minimise the anode erosion due to limited motions of arc root. Indeed, anode erosion occurs due to the strong heat fluxes of the constricted arc attachment between the arc

column and the anode surface. Bobzin *et al*. [19] identified a preferential arc attachment spot for an argon-hydrogen mixture with a cascaded-anode plasma torch. They proposed to control the electric arc movement on the anode wall by applying an external magnetic field by the use of magnets. Zhukovskii *et al*. [20] also simulated the application of various strength of an external magnetic field to reduce anode erosion.

Although instabilities are reduced with cascaded-anode plasma torch, it is interesting to study electric arc behaviour since it will influence particle treatment as explained above [14, 16, 21] and anode erosion [5, 22]. Indeed, Leblanc *et al.* [23] showed that the state of in-flight particle (temperature and velocity) significantly varies with spraying time with a conventional plasma torch due to electrodes erosion. A difference of 200 °C and 25 m/s is observed for particles temperature and velocity after approximately 45 hours of spraying, leading to a variation in coatings porosity.

However, the arc observation inside the torch remains challenging because of the torch design, high temperature and radiation. End-on imaging of the arc confined within the torch provides significant information about the arc dynamics. For example, Dorier *et al*. [22] studied the fluctuating behaviour of a conventional plasma torch (F4 from Sulzer Metco) by synchronizing arc voltage measurement and end-on imaging. They observed multiple attachments at least during 1 µs (camera exposure time) due to succession of arc roots formation and vanishing. The existence of multiple arc roots was also highlighted by Ghorui *et al*. [24] and Qiang *et al*. [25] in a direct current non-transferred arc plasma torch. The possibility for theses arc roots to move along the anode surface leads to important voltage fluctuations.

The aim of this paper is to highlight the influence of plasma forming gases composition on the electric arc dynamics, especially its anodic attachment. The study of electric arc dynamics greatly contributes to the process understanding and to the control of coating properties. To the authors knowledge, synchronized end-on imaging of the arc on a cascaded-anode plasma torch has not been yet reported and is studied in this paper. The following section describes the

diagnostics devices used and the experimental conditions studied. Then, anodic arc roots observations are presented and discussed for different plasma forming gas compositions. The last section gives the conclusion.

2. Experimental set-up

2.1. Plasma torch and diagnostics devices

The plasma torch used here is SinplexPro™ from Oerlikon Metco with an anode nozzle diameter of 9 mm. The diagnostics devices are illustrated in Fig. 2. While the arc current and voltage are monitored, two J-type thermocouples measure temperature variation ΔT in cooling water system between the anode and the cathode. In order to quantify Q_{loss}, the heat lost to the torch cooling water, equation *(1)* is used:

$$Q_{loss} = \dot{m}_w c_p \Delta T \qquad (1)$$

where $\dot{m}_w$ is the water mass flow rate in kg.s^{-1} ($\dot{m}_w$ = 0.34 kg.s^{-1}) and c_p the specific heat of water in J.kg^{-1}.K^{-1} (c_p = 4 184 J.kg^{-1}.K^{-1}). Then, plasma torch thermal efficiency η can be determined thanks to equation *(2)*:

$$\eta = 1 - \frac{Q_{loss}}{UI} \qquad (2)$$

where U and I are respectively the arc voltage in V and the current intensity in A.

The device allows measuring voltage fluctuations between the anode and the cathode thanks to a differential probe 1/20 (METRIX MX9030Z, 30 MHz bandwidth, ± 600 V, accuracy ± 3%). The voltage signals were recorded by LabVIEW software thanks to a data acquisition unit. The LabVIEW program runs with a sampling rate of 1.5 MHz. Each measurement records 100 000 samples and 1 000 measurements are carried out in order to calculate the mean voltage $\overline{U}$ and the voltage fluctuation (VF) defined by equation *(3)*:

$$VF = \frac{2\sigma}{\overline{U}} \qquad (3)$$

where σ is the standard deviation in V and VF is expressed in percentage.

The program also uses a Fast Fourier Transform (FFT) method to perform a frequency analysis in order to identify characteristic frequency peaks. Note that the power supply regulates the electrical current at a frequency of 60 kHz which generates harmonics on voltage spectra.

Optical emission spectroscopy (HRS 2 Jobin Yvon spectrometer) was used to study plasma jet brightness fluctuations. An optical fiber is placed at 5 mm from the nozzle exit and a photomultiplier (R928 Hamamatsu) converts the light signal into an electrical signal. The Ar I line located at 420 nm was followed because of its high relative intensity [26].

A mirror and an intensified 16 bit camera (pco.dicam C1) equipped with a Questar QM1 lens were used for imaging of the nozzle interior. Frame rate was set to 120 frames per second and different exposure times were compared. In order to successfully observe arc root shape and location, a mask is required to attenuate the light emitted by the arc column and the cathode. The masking issue is discussed in the following section since a compromise has to be found between mask diameter and exposure time.

2.2. Masking issue

Direct photography was used by Li *et al.* [27] in order to observe arc roots, but the obtained images do not allow clearly identifying arc roots location. The light emitted from the high-temperature arc column is very intense and interferes with arc root observations. This phenomenon can be explained by the difference in radiative emissions between the plasma core and the plasma edge at the anode wall. Assuming that the plasma is isothermal and assimilated to a sphere of radius R_p, the net emission coefficient ε can be defined, for a given pressure, as $\varepsilon(T, R_p) = \int_0^\infty L_\lambda^0(T) K_\lambda(T) e^{(-K_\lambda(T) R_p)} d\lambda$, where L_λ^0 is the spectral radiation intensity of a black body and K_λ is the spectral absorption coefficient at the wavelength λ [28]. The net emission coefficient radial profile for pure argon is presented in Fig. 3, where the temperature profile is taken from [29] and the radiation properties are used from [30]. Five orders of magnitude in the

radiation emission between the axis ($r = 0$) and the anode wall ($r = 4.5$ mm) can be highlighted. It means that masking the plasma core is necessary to focus on the plasma edges where the arc reattaches at the anode wall and to avoid camera saturation.

Captured images are in grey scale, which means that each point is represented by a brightness value, ranging from 0 (black) to 65 535 (white), with intermediate value representing different levels of grey. A shade 8 optical filter with a transmittance of 10 % in the visible spectral range (according to EN 169) was used to reduce light signal. From Fig. 3, the lowest value of brightness (0) can be set at 10^5 W.m^{-2}. Then, the highest value (65 535) should not exceed 6.55×10^9 W.m^{-2}. Since only 10 % of the signal is transmitted, the maximum brightness is 6.55×10^8 W.m^{-2}, which corresponds to the horizontal dotted line. The theoretical light intensity profile permits to identify a mask radius of about 3 mm to successfully observe anodic arc attachments. This size of the mask has been validated by observations of the nozzle interior as explained below.

First, nozzle observations were carried out with an exposure time of 6.5 ms for an argon-hydrogen mixture with a shade 8 optical filter to avoid image saturation and sensor damage. Fig. 4 A is an example of one image obtained at 500 A. The white ring delimits the nozzle wall and the luminous area in the center corresponds to the light emitted by the arc column. This type of images can be used to estimate the thickness of the cold boundary layer (CBL). For example, Kim *et al*. [31] defined the arc column width as the location where the light intensity has dropped to 90 % of its maximum value. In [10, 32], this criterion is set a 50 % of the maximum value. In this paper, images were used to define a layer between the arc column and the anode wall called « $I_{max}/2$-layer ». The thickness dependence on plasma forming gases will be highlighted in the following. Note that it does not correspond to the layer usually named « cold boundary layer (CBL) » since it is difficult to identify it on end-on images, but this layer contains the CBL.

To estimate the $I_{max}/2$-layer thickness, a horizontal line is drawn crossing the arc column center (coloured in orange in Fig. 4 A), the light intensity is measured along this line and a light intensity profile is obtained (Fig. 4 B). The $I_{max}/2$-layer is located between the point where light intensity if half of the highest one and the nozzle wall.

It is difficult to clearly identify arc roots in Fig. 4 A, but thanks to edge detection (selection of pixels with the same grey level) it is possible to highlight one arc root in the lower area of the nozzle (Fig. 4 C). This permits to identify an area that needs to be hidden, represented by the red ring in Fig. 4 D, whose diameter is approximately 6 mm as identified thanks to light intensity profile (Fig. 3). Masking nozzle centre will allow performing end-on imaging without filter and with reduced exposure time to observe arc roots dynamics, with no saturation issue.

Fig. 5 comprises two images of anodic arc root attachment with mask captured with two different exposure times: 150 ns (Fig. 5 A) and 60 ns (Fig. 5 B) for an argon-hydrogen mixture at 500 A. In both images, one arc root is located in the lower area of the nozzle which is more visible than in Fig. 4 A. However, when exposure time is set at 150 ns, there are more luminous noises corresponding to light diffusion by the anode wall. A shorter exposure time limits the light captured by the sensor and the anodic arc roots are more visible. Moreover, it allows observing their fast dynamics and possibly characterizing multiple arc attachments. Thereby, end-on images that are next presented were captured with an exposure time of 60 ns and a mask diameter of 6 mm for all operating conditions.

2.3. Experimental conditions

A plasma gas mixture is characterized by its thermodynamic properties such as mass enthalpy and specific heat and transport properties (viscosity, thermal and electrical conductivities). Three main gases are widely used in plasma spraying: argon, hydrogen and helium. Due to its high molecular weight, Argon gas allows a good transfer of momentum to the particles and provides velocity to the plasma jet. Hydrogen permits to increase the plasma specific enthalpy

and thermal conductivity, and improves the heat transfer to the particles. Plasma gas viscosity depends on interactions between species that are present in the plasma. As helium ionisation occurs at high temperature (> 13 000 K), presence of non-ionized He atoms will lead to a high plasma gas viscosity at temperature higher than 10 000 K. Therefore, engulfment of surrounding cold air is limited with helium. Mixtures of theses gases are usually used to combine these properties. In this study, three plasma forming gas composition were studied: pure argon, argon-hydrogen mixture and argon-helium mixture. A flow rate of 50 slpm of argon was selected according to the operating limits recommended by the manufacturer [33]. In order to evaluate the influence of the addition of hydrogen and helium to argon, mixtures rich in secondary gases were selected. For Ar-H_2 mixture, a flow rate of 12 slpm of H_2 was added to 50 slpm of Ar, which is near the maximum hydrogen flow recommended [33]. For Ar-He mixture, 55 slpm of He is added to 43 slpm of Ar to not exceed a total flow rate of 100 slpm and in order to have approximately the same total mass flow rate for the three conditions (about 1.5 $g.s^{-1}$). Current intensity was fixed at 500 A and Table I summarizes experimental conditions.

3. Results and discussion

3.1. Plasma torch ignition

During plasma torch ignition, anode erosion can occur and some preferential attachments can be created. Here, the very first ignition with brand-new electrodes was observed. Fig. 6 depicts the time evolution of current and voltage during plasma torch ignition. Note that these data have been extracted from the commercial control system which makes a measurement every second. First, it can be noticed that it takes approximately 10 seconds for voltage and current to stabilize at the desired current.

Fig. 7 A shows a succession of images (about 8.3 ms separates each frame) during first plasma torch ignition corresponding to the very first ms (duration of 75 ms) when electrical power is

still low. In order to highlight anodic arc roots, images have been binarized (based on an auto-thresholding), therefore, light intensity cannot be compared with images presented further.

At least there are two constricted anodic arc roots simultaneously during 60 ns. One seems to move very slightly on the left-hand side (Fig. 7 A, green arrow in frame 1) while the second one is continually rotating on the anode surface (Fig. 7 A, yellow arrows).

Fig. 7 B presents a succession of six images after about 2 seconds of ignition, when arc voltage had increased to approximately 55 V. Anodic arc root on the left-hand side of the anode (pointed by the green arrow in frame 1) is still present and seems to be stationary. Two additional arc roots are observed. The second one is pointed by the red arrow in Fig. 7 B frame 1 and is not moving on the anode wall. It keeps up anchoring on the right-hand side but with a lower intensity than that fixed on the opposite side. The third one (yellow arrows in Fig. 7 B) is located on the top of the anode wall in frame 1, and gradually disappears and reappears in the following frames.

It seems that, while electrical power increases, stabilization of one main arc root on the left-hand side of the anode occurs. A second arc root on the right-hand side appears with a lower light intensity suggesting that the arc current passing through it may be lower.

It has to be underlined that the automatic procedure of plasma ignition by the commercial system gives rise to a constant injection volume flow rate of argon of 70 slpm. Once the arc voltage and current are stabilized, the desired composition of plasma gases is injected and the electric arc dynamic can change.

3.2. Influence of plasma forming gas composition on arc attachment

Anodic arc root observations were carried out for three plasma forming gas composition: argon, argon-hydrogen and argon-helium. Videos shared as supplementary materials are a succession of 100 images for each condition. In this section, successions of images are presented and discussed. To facilitate arc root visualisation, ImageJ software has been used to change grey

scale images in pseudo-colour images via a lookup table. Differences in colour in pseudo-coloured images reflect differences in intensity of the original image. Thus, intensity of pseudo-coloured images for each condition can be compared.

Fig. 8 is a succession of nine images for pure argon plasma. It shows that there is an area more luminous on upper left-hand side of the anode wall, which may correspond to the stable anodic arc root as seen during plasma torch ignition. A second anodic arc root can be observed (highlighted by yellow arrow in frame 3) only in a few frames on lower right-hand side of the anode wall. Video of arc root dynamics for pure argon corroborates these observations and highlights the movement of the second anodic arc root, appearing and disappearing continuously on lower right-hand side of the anode wall.

In comparison, Fig. 9 represents anodic arc roots observations for argon-hydrogen mixture. It shows multiple luminous areas all around the anode wall, corresponding to multiple reattachments (highlighted by yellow arrows in several frames). These multiple reattachments are clearly visible on the video and a circular movement of these arc roots can be observed. Video shows also a main arc root stabilized on upper left-hand side of the anode wall, as for pure argon plasma. Moreover, plasma light intensity is higher than for pure argon plasma.

For the third plasma gas composition, Fig. 10 shows that argon-helium plasma leads to a lower plasma light intensity than pure argon plasma or argon-hydrogen mixture. As for Ar-H_2 mixture, some reattachments occur (frames 4 and 7) and up to three anodic arc roots are observed simultaneously (frame 5). Lower plasma light intensity makes it more difficult to observe arc root dynamics on video but still a higher number of reattachments are observable than for pure argon plasma.

Different electric arc dynamics have been observed with these three gas compositions. The addition of hydrogen leads to a higher energy plasma due to H_2 dissociation at about 3 500 K [34] and could explain the higher plasma light intensity for the argon-hydrogen mixture. An assumption is made further about the less radiative plasma when He is added.

As a partial conclusion, end-on imaging was used to observe how plasma forming gases influence arc roots dynamics. Videos shared as supplementary materials and Fig. 8, 9 and 10 highlighted one stable anodic arc root on the upper left-hand side of the anode wall for the three experimental condition, which may correspond to the one observed during plasma torch ignition. The addition of a secondary plasma forming gas has an influence on plasma light intensity and on the number of reattachments that occur. These different behaviours can be explained by examining the thermal balances for each condition.

Mean voltages for the three conditions are presented in Fig. 11 A and are comprised between 67 and 89 V. The highest value is obtained for argon-hydrogen mixture and the lowest for pure argon plasma. This can be explained by thermal properties of these mixtures, particularly their thermal conductivity [35]. Fig. 11 B shows that it is higher for argon-hydrogen and argon-helium than for pure argon. Indeed, an increase in thermal conductivity is followed by a reduction in electric arc radius because heat exchanges between the arc and the surrounding cold gas are more efficient [3, 36]. Arc column constriction occurs and leads to an increase in the electric field and thus in the arc voltage.

A warmer cold boundary layer for argon-hydrogen and argon-helium is expected and could explain the higher number of reattachments for these two mixtures observed in the videos compared with pure argon. Indeed, the arc column strikes the anode wall when the cold boundary layer temperature is high enough [37].

Table II reports the standard deviation of arc voltage, the percentage of voltage fluctuations, the specific enthalpy and the $I_{max}/2$-layer thickness for each condition. The latter is expressed in nozzle diameter percentage and was measured 5 times for each condition from end-on images without masking, as explained in Fig. 4 B. Voltage signals and frequency spectra (for voltage and plasma jet fluctuations) are also presented in Fig. 12.

Table II reports very low voltage fluctuations for the three conditions (maximum 1 %) compared with large voltage fluctuations that are measured in a conventional plasma torch (≥ 70 %) [38]. Here, the argon-hydrogen mixture is characterized by the lowest voltage fluctuation (0.3 %) compared with pure argon and argon-helium mixture (about 1 %). This behaviour is quite different from a conventional plasma torch one. Indeed, it has been shown that the addition of hydrogen significantly increases voltage fluctuation with an F4 plasma torch because the resulting increase in cold boundary layer thickness promotes the upstream large scale shunting process of the arc [32]. In the cascaded-anode torch, the arc attachment is constrained by the neutrodes stacking to be localized on a shorter area limiting the shunting process. Moreover, argon-hydrogen mixture shows the lowest voltage fluctuation despite the fact that anodic arc roots are in a circular movement. The assumption here is that the observed reattachments may occur in a same vertical plan where heat is intensively deposited, so that the arc length and the electric field are quite the same.

Figure 12 comprises voltage signals for the three plasma forming gas compositions (Fig. 12 A) and both voltage and brightness spectra for pure argon (Fig. 12 B), argon-hydrogen mixture (Fig. 12 C) and argon-helium mixture (Fig. 12 D). Voltage signals present a high fluctuation frequency (60 kHz) due to power supply regulation as explained in the experimental set-up section, which induces the presence of harmonics on voltage spectra, particularly for pure argon plasma (Fig. 12 B). Peaks are observed at low frequency (2.4 kHz for pure argon, 2.8 kHz for argon-hydrogen mixture and 3.2 kHz or argon-helium mixture). As shown by voltage signals (Fig. 12 A), intensity of this low frequency fluctuation is higher for Ar-He mixture (about 10^{-4} a.u. compared to 10^{-6} a.u. for Ar-H_2 mixture). With a conventional plasma torch, Janisson [3] observed an increase in fluctuation frequency when helium is added (from 8 kHz to 13 kHz for a volume percentage of He varying from 0 to 60 % at 460 A). Here, cascaded-anode plasma torch behaves differently with an increase in peak intensity for this experimental condition.

For the three plasma forming gas compositions, the low voltage fluctuation frequency around 3 kHz is also observed on brightness spectra which means that these fluctuations could have an impact on in-flight particle treatment. In brightness spectra, additional peaks are present at higher frequency, 11 kHz for pure argon, 30 kHz for argon-hydrogen mixture and 15 and 20 kHz for argon-helium mixture. The origin of these fluctuations is still unknown but due to their high frequency occurrence, but their impact on in-flight particle treatment should be limited.

A singular behaviour of argon-helium mixture is also observed with the study of thermal balance. In Fig. 13 are represented the heat losses in the cooling water (in kW) and the thermal efficiency (in %) calculated by equations *(1)* and *(2)*. Thermal efficiency is comprised between 44 % and 83 %. The argon-hydrogen mixture leads to significant heat losses due to higher electrical power resulting in a warmer plasma gas near the anode wall. Indeed, the $I_{max}/2$-layer thickness is lower for this mixture (see Table II), leading to higher heat losses. Hence, plasma torch thermal efficiency is the lowest for that mixture. On the contrary, plasma torch operating with an argon-helium mixture is characterized by a high thermal efficiency (more than 80 %) due to very low heat losses for that mixture (6.6 kW against 14.8 kW for pure argon and 25.1 kW for argon-hydrogen mixture). The $I_{max}/2$-layer for Ar-He mixture is thicker (23.2 %) which limits heat exchange between the anode wall and the arc column.

The heat losses have different origins: electric losses at the arc attachment, conducto-convective losses between arc column and plasma forming gas, and radiative losses due to plasma radiation [39]. The power received by neutrodes and anode (convective and conductive phenomena) can be expressed with the following equation *(4)*:

$$Q_c = 2\pi r L q_{wall} \text{ with } q_{wall} = -\kappa \left(\frac{dT}{dr}\right)_{wall} \qquad (4)$$

where r is the anode radius and L the total length of neutrode and anode, and q_{wall} is approximated by Fourier's law (κ is the thermal conductivity of the plasma gas and $\left(\frac{dT}{dr}\right)_{wall}$ the thermal gradient at the anode wall). The higher thermal conductivity of argon-helium mixture

does not explain the low heat losses for that mixture. The assumption here is that the second term of the equation, the thermal gradient at the anode wall, may be lower in argon-helium mixture. It is worth underlining that the addition of helium to argon leads to decrease the electrical conductivity of the arc, shifting to higher temperatures the electrical conduction threshold and therefore reducing the Joule heating in the cold boundary layer. Imaging of the nozzle interior supports this assumption since the plasma light intensity is lower when helium is added (Fig. 14). Indeed, the enthalpy profile may be sharper for argon-helium mixture, leading to low heat losses to the anode wall.

Another point to consider is the radiative losses. At 500 A, radiation contribution is expected to be high, and the comparison of net emission coefficients for pure argon and for argon-helium mixture shows that it is lower for pure helium than for pure argon [40]. In this paper, the composition of the argon-helium mixture studied is about 44 vol.% of argon and 56 vol.% of helium, near the composition 50-50 % studied in [40]. Determination of mean specific enthalpy (Table II) allows determining an average temperature thanks to thermal properties of gases ($h = f(T)$ curves [35]). The value obtained is about 12 200 K for pure argon and 12 600 K for argon-helium mixture. From [40], net emission coefficients are approximately 1.5×10^8 W.m^{-3}.sr^{-1} for pure argon and 1.2×10^8 W.m^{-3}.sr^{-1} for argon-helium mixture. Radiative losses for argon-helium mixture are therefore slightly lower than pure argon. This phenomenon associated with the low thermal gradient and thicker $I_{max}/2$-layer may explain the low heat losses obtained for this mixture.

4. Conclusions

The study of the electric arc dynamics is important since it will influence plasma jet stability and anode erosion. This paper focuses on one operating condition with the same mass flow rate and the same current intensity in order to understand the influence of plasma forming gas

composition on the electric arc behaviour in SinplexPro^{TM}, commercial cascaded-anode plasma torch. Three different compositions were studied: argon, argon-hydrogen, and argon-helium. Multiple constricted arc roots were observed during plasma torch ignition and in steady state for all experimental conditions. A preferential attachment zone on the left-hand side of the anode wall has been identified, independently of anode erosion since it was brand-new when we first observed this stabilization. The addition of a secondary plasma gas leads to a higher number of reattachments compared with pure argon.

The Ar-H_2 mixture is characterized by a very low voltage fluctuation percentage (0.3 %). The higher thermal conductivity of this mixture leads to a warmer cold boundary layer and can explain the higher number of reattachments observed in the video. These reattachments can occur in a same vertical plan where heat is intensively deposited, resulting in very low voltage fluctuations.

A singular behaviour has been identified when helium is added as a secondary plasma forming gas. Very high thermal efficiency can be obtained (about 80 %) and a characteristic frequency peak is obtained around 3 kHz on the frequency spectrum. The Ar-He mixture has a high thermal conductivity but since helium ionization energy is important, the electrical conductivity in the cold boundary layer is reduced, resulting in lower Joule heating. The thermal gradient at the anode wall could be lower in argon-helium mixture. Temperature and velocity profiles at the torch end need to be determined to validate this assumption.

The behaviour of a cascaded-anode plasma torch is very different from a conventional one: very low amplitudes of voltage fluctuations were obtained (about 1 %) and the addition of H_2 led to the lowest voltage fluctuations percentage between the compositions studied in this paper with SinplexPro^{TM}. These fluctuations are due to the electric arc movement and influence the plasma jet stability as shown by the study of plasma jet brightness fluctuations. Therefore, in-flight particle characteristics (temperature and velocity) and coating properties should be affected.

This work will help to understand how a cascaded-anode plasma torch is operating. It will also allow following the anode erosion process, directly link to the type of attachment of the anodic arc root (constricted, diffused). Indeed, the multiple arc roots observed during plasma torch ignition and the stabilization of one main arc root may lead to erosion processes, damaging the anode surface. The erosion issue will be discussed in a future work by comparing the electric arc movement in two different nozzle diameters (9 mm and 6.5 mm).

List of references

[1] Vardelle, A.; Moreau, C.; Themelis, N.J. and Chazelas, C.: A perspective on plasma spray technology, Plasma Chemistry and Plasma Processing, **35** (2015), no. 3, pp. 491–509.

[2] Fauchais, P. and Vardelle, M.: Plasma spraying: present and future, Pure and Applied Chemistry, **66** (1994), no. 6, pp. 1247–1258.

[3] Janisson, S.: Study of plasma jets and particles treatment in plasma spraying with ternary gas mixture in controlled atmosphere and temperature, PhD Thesis (in french), University of Limoges, France, 1999.

[4] Heimann, R.B.: Plasma spray coating, principles and applications, Plasma spray coating, principles and applications ed., Wiley VCH, 1996.

[5] Planche, M.P.: Study of the fluctuations in a DC plasma torch. Application to the dynamic behaviour of the arc and to the measurements of the flow velocity, PhD Thesis (in french), University of Limoges, France, 1995.

[6] Heberlein, J.; Mentel, J. and Pfender, E.: The anode region of electric arcs: a survey, Journal of Physics D: Applied Physics, **43** (2010), no. 2, p. 023001.

[7] Fauchais, P.; Heberlein, J. and Boulos, M.: Thermal spray fundamentals, Springer US, Boston, MA, 2014.

[8] Wutzke, S.A.; Pfender, E. and Eckert, E.R.G.: Study of electric arc behavior with superimposed flow., American Institute of Aeronautics and Astronautics, **5** (1967), no. 4, pp. 707–714.

[9] Fauchais, P. and Vardelle, A.: Thermal plasmas, IEEE Transactions on Plasma Science, **25** (1997), no. 6.

[10] Duan, Z. and Heberlein, J.: Arc instabilities in a plasma spray torch, Journal of Thermal Spray Technology, **11** (2002), no. 1, pp. 44–51.

[11] Rat, V.; Mavier, F. and Coudert, J.F.: Electric arc fluctuations in DC plasma spray torch, Plasma Chemistry and Plasma Processing, **37** (2017), no. 3, pp. 549–580.

[12] Coudert, J.F.; Rat, V. and Rigot, D.: Influence of Helmholtz oscillations on arc voltage fluctuations in a dc plasma spraying torch, Journal of Physics D: Applied Physics, **40** (2007), no. 23, pp. 7357–7366.

[13] Coudert, J.F. and Rat, V.: Influence of configuration and operating conditions on the electric arc instabilities of a plasma spray torch: role of acoustic resonance, Journal of Physics D: Applied Physics, **41** (2008), no. 20, p. 205208.

[14] Bisson, J.F.; Gauthier, B. and Moreau, C.: Effect of plasma fluctuations on in-flight particle parameters, Journal of Thermal Spray Technology, **12** (2003), no. 1, pp. 38–43.

[15] Goutier, S.; Noguès-Delbos, E.; Vardelle, M. and Fauchais, P.: Particle temperature fluctuations in plasma spraying, Journal of Thermal Spray Technology, **17** (2008), nos. 5–6, pp. 895–901.

[16] Bisson, J.F. and Moreau, C.: Effect of direct-current plasma fluctuations on in-flight particle parameters: Part II, Journal of Thermal Spray Technology, **12** (2003), no. 2, pp. 258–264.

[17] Zhukov, M.F. ed.: Thermal plasma torches: design, characteristics, applications, Cambridge International Science Publ, Cambridge, 2007.

[18] Seshadri, R.C. and Sampath, S.: Characteristics of conventional and cascaded arc plasma spray-deposited ceramic under standard and high-throughput conditions, Journal of Thermal Spray Technology, **28** (2019), no. 4, pp. 690–705.

[19] Bobzin, K.; Öte, M.; Knoch, M.A.; Heinemann, H.; Zimmermann, S. and Schein, J.: Influence of external magnetic fields on the coatings of a cascaded plasma generator, IOP Conference Series: Materials Science and Engineering, **480** (2019), p. 012004.

[20] Zhukovskii, R.; Chazelas, C.; Vardelle, A. and Rat, V.: Control of the arc motion in DC plasma spray torch with a cascaded anode, Journal of Thermal Spray Technology, **29** (2020), nos. 1–2, pp. 3–12.

[21] Fauchais, P.; Montavon, G.; Vardelle, M. and Cedelle, J.: Developments in direct current plasma spraying, Surface and Coatings Technology, **201** (2006), no. 5, pp. 1908–1921.

[22] Dorier, J.-L.; Gindrat, M.; Hollenstein, C.; Salito, A.; Loch, M. and Barbezat, G.: Time-resolved imaging of anodic arc root behavior during fluctuations of a DC plasma spraying torch, IEEE Transactions on Plasma Science, **29** (2001), no. 3, pp. 494–501.

[23] Leblanc, L. and Moreau, C.: The long-term stability of plasma spraying, Journal of Thermal Spray Technology, **11** (2002), no. 3, pp. 380–386.

[24] Ghorui, S.; Tiwari, N.; Meher, K.C.; Jan, A.; Bhat, A. and Sahasrabudhe, S.N.: Direct probing of anode arc root dynamics and voltage instability in a dc non-transferred arc plasma jet, Plasma Sources Science and Technology, **24** (2015), no. 6, p. 065003.

[25] Qiang, S.; Yonghong, L.; Yancong, H.; Xinlei, W.; Peng, L. and Hui, J.: A novel experimental method of investigating anode-arc-root behaviors in a DC non-transferred arc plasma torch, Plasma Sources Science and Technology, **29** (2020), no. 2, p. 025008.

[26] National Institute of Standards and Technology, https://www.nist.gov/pml/atomic-spectroscopy-databases.

[27] Li, H.; Ma, Q.; Li and Xia, W.D.: Imaging of behavior of multiarc roots of cathode in a dc arc discharge, IEEE Transactions on Plasma Science, **33** (2005), no. 2, pp. 404–405.

[28] Hermette, L.; Cressault, Y.; Gleizes, A.; Jan, C. and Bousoltane, K.: Radiative properties of SF6-C2F4-Cu mixtures in High Voltage Circuit Breakers Arc Plasmas: Net Emission Coefficient and mixing rules, 2014.

[29] Zhukovskii, R.; Chazelas, C.; Rat, V.; Vardelle, A. and Molz, R.: Model of a non-transferred arc cascaded-anode plasma torch: the two-temperature formulation, Journal of Physics D: Applied Physics, **55** (2022), no. 6, p. 065202.

[30] Erraki, A.: Study of radiative transfer in thermal plasmas: application to SF6 and argon-iron mixture, PhD Thesis (in french), University of Toulouse III, France, 1999.

[31] Kim, S.; Heberlein, J.; Lindsay, J. and Peters, J.: Methods to evaluate arc stability in plasma arc cutting torches, Journal of Physics D: Applied Physics, **43** (2010), no. 50, p. 505202.

[32] Nogues, E.; Fauchais, P.; Vardelle, M. and Granger, P.: Relation between the arc-root fluctuations, the cold boundary layer thickness and the particle thermal treatment, Journal of Thermal Spray Technology, **16** (2007), nos. 5–6, pp. 919–926.

[33] Oerlikon Metco: SinplexProTM plasma spray gun product manual, 2018.

[34] Boulos, M.I.; Fauchais, P. and Pfender, E.: Thermal plasmas, Springer US, Boston, MA, 1994.

[35] CEA, French Alternative Energies and Atomic Energy Commission: Calculation of thermal and transport properties, 2021.

[36] Planche, M.P.; Coudert, J.F. and Fauchais, P.: Velocity measurements for arc jets produced by a DC plasma spray torch, Plasma Chemistry and Plasma Processing, **18** (1998), no. 2, pp. 263–283.

[37] Fauchais, P.: Understanding plasma spraying, Journal of Physics D: Applied Physics, **37** (2004), no. 9, pp. R86–R108.

[38] Nogues, E.; Vardelle, M.; Fauchais, P. and Granger, P.: Arc voltage fluctuations: comparison between two plasma torch types, Surface and Coatings Technology, **202** (2008), no. 18, pp. 4387–4393.

[39] Rat, V.; Krowka, J. and Coudert, J.F.: Enthalpy modulation of a laminar pulsed nitrogen arc jet: time-resolved diagnostics and model, Plasma Sources Science and Technology, **24** (2015), no. 4, p. 045009.

[40] Cressault, Y.; Rouffet, M.E.; Gleizes, A. and Meillot, E.: Net emission of Ar–H_2–He thermal plasmas at atmospheric pressure, Journal of Physics D: Applied Physics, **43** (2010), no. 33, p. 335204.

Tables

Table I: Experimental conditions studied.

Plasma forming gas	Flow rate (slpm)	Vol.%	Total mass flow rate ($g.s^{-1}$)	Current (A)
Ar	50	100 vol.% Ar	1,49	
Ar-H_2	50-12	19 vol.% H_2	1,50	500
Ar-He	43-55	56 vol.% He	1,44	

Table II: Standard deviation, voltage fluctuation, specific enthalpy and $I_{max}/2$-layer thickness for each experimental condition

Plasma forming gas	Vol.%	Mean voltage (V)	Standard deviation (V)	Voltage fluctuation (%)	Specific enthalpy ($MJ.kg^{-1}$)	$I_{max}/2$-layer (%)
Ar	100 vol.% Ar	67	0.3	1	12,6	20.7
Ar-H_2	19 vol.% H_2	89	0.2	0.3	13	20.3
Ar-He	56 vol.% He	79	0.4	1.1	22,8	23.2

List of figure captions

Fig. 1: Simplified scheme of A) a conventional plasma torch and B) a cascaded-anode plasma torch.

Fig. 2: Diagnostics devices for measuring and recording thermal balances, arc voltage fluctuations, plasma jet brightness fluctuations and anodic arc root observations.

Fig. 3: Net emission coefficient radial profile for pure argon at 500 A.

Fig. 4: Example of one image obtained with the intensified camera for an Ar-H_2 mixture at 500 A, A) nozzle wall delimitation and horizontal line to measure the light intensity, B) normalized light intensity profile and « $I_{max}/2$-layer » measurement, C) edge detection to highlight arc root and D) identification of an area to hide (red circle) thanks to edge detection in orange.

Fig. 5: Image captured with two different exposure times for an Ar-H_2 mixture at 500 A: A) 150 ns and B) 60 ns. Frame rate: 120 fps, exposure time: 60 ns.

Fig. 6: Time evolution of current and voltage during plasma torch ignition.

Fig. 7: Succession of end-on images during plasma torch ignition with new electrodes: A) at the very beginning and B) after 2 seconds of ignition.

Fig. 7: Succession of 9 images of nozzle interior for pure argon plasma. Frame rate: 120 fps, exposure time: 60 ns.

Fig. 8: Succession of 9 images of nozzle interior for an argon-hydrogen mixture. Frame rate: 120 fps, exposure time: 60 ns.

Fig. 9: Succession of 9 images of nozzle interior for an argon-helium mixture. Frame rate: 120 fps, exposure time: 60 ns.

Fig. 10: A) Mean voltage measured at the torch end and B) evolution of thermal conductivity for each experimental condition.

Fig. 11: A) Voltage signals and voltage and brightness frequency spectra for B) pure Ar, C) Ar-H_2 mixture and D) Ar-He mixture.

Fig. 12: Thermal efficiency and heat losses in the torch cooling water.

Fig. 13: Comparison of the light intensity inside the anode for pure argon and an argon-helium mixture. Frame rate: 120 fps, exposure time: 60 ns.

Figures

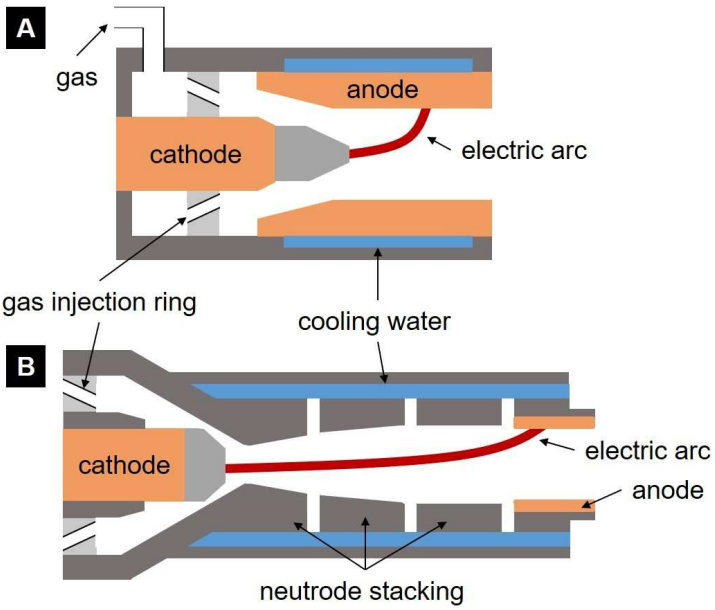

Figure 1

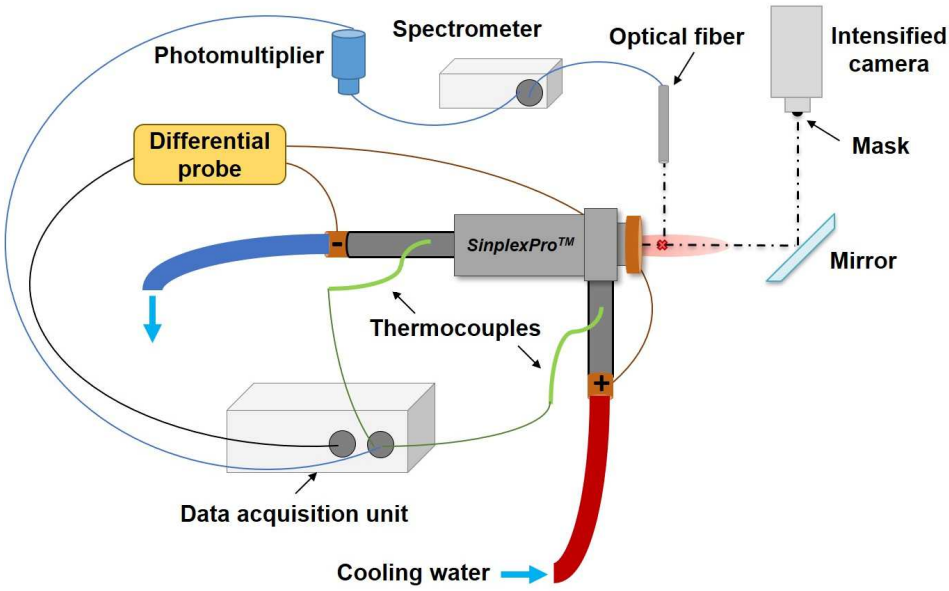

Figure 2

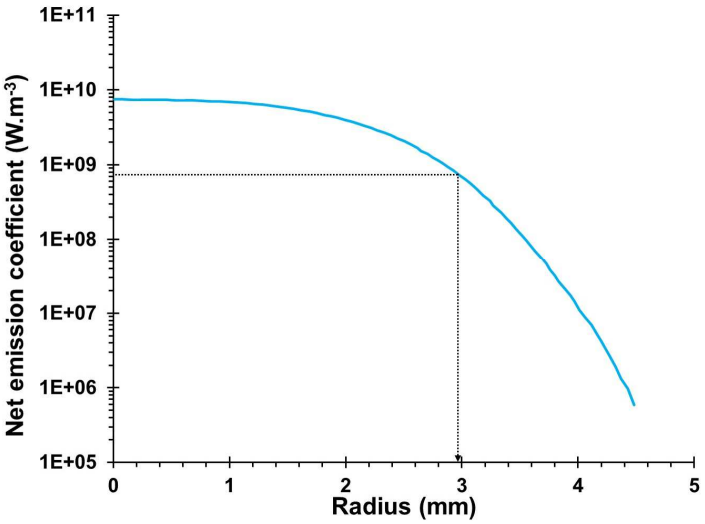

Figure 3

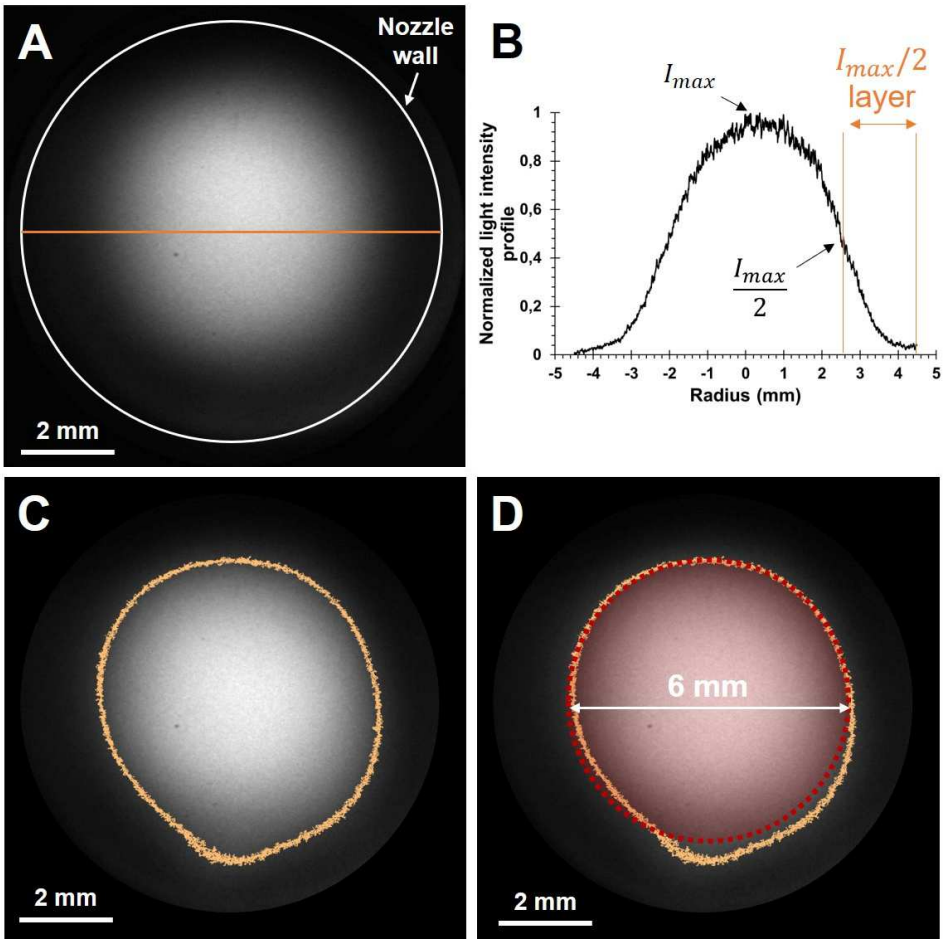

Figure 4

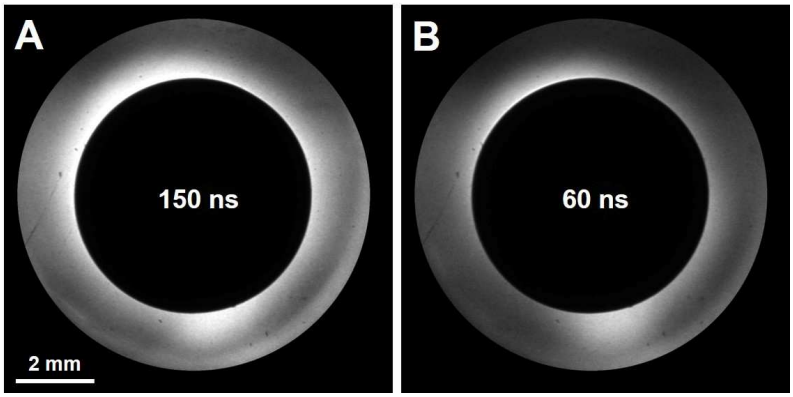

Figure 5

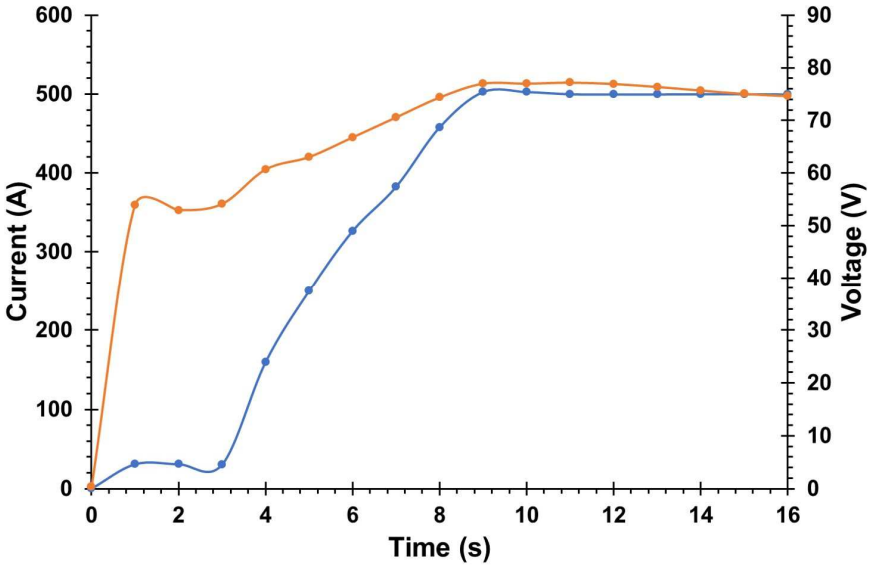

Figure 6

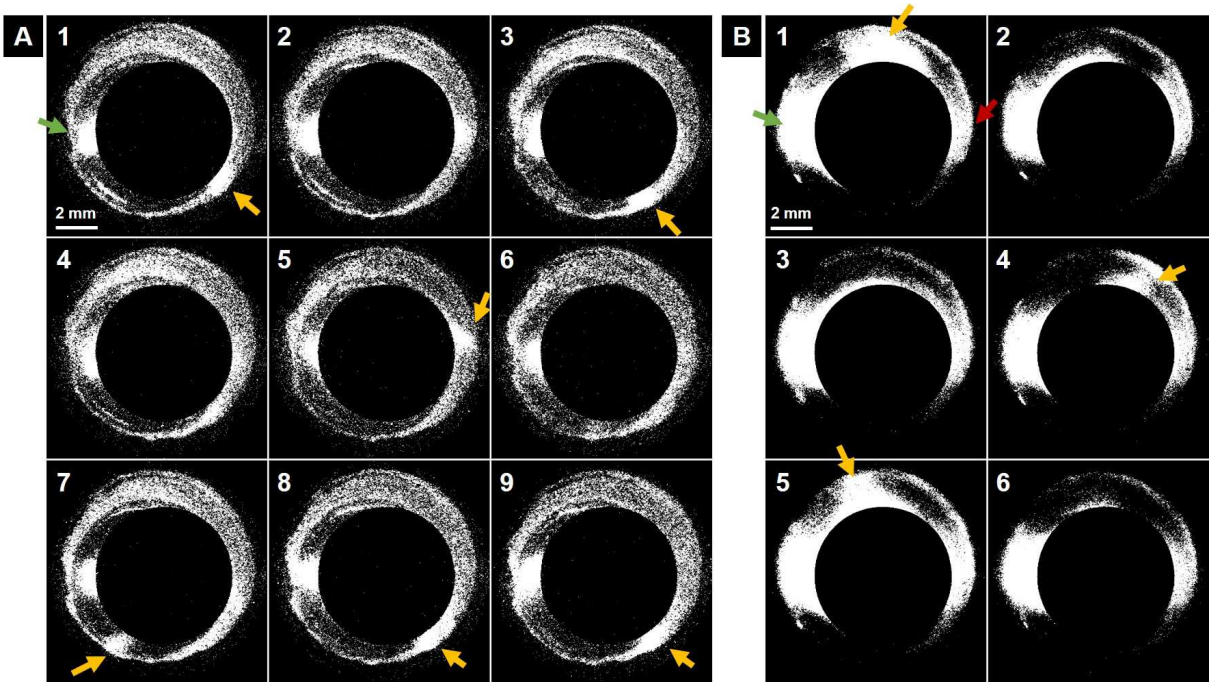

Figure 7

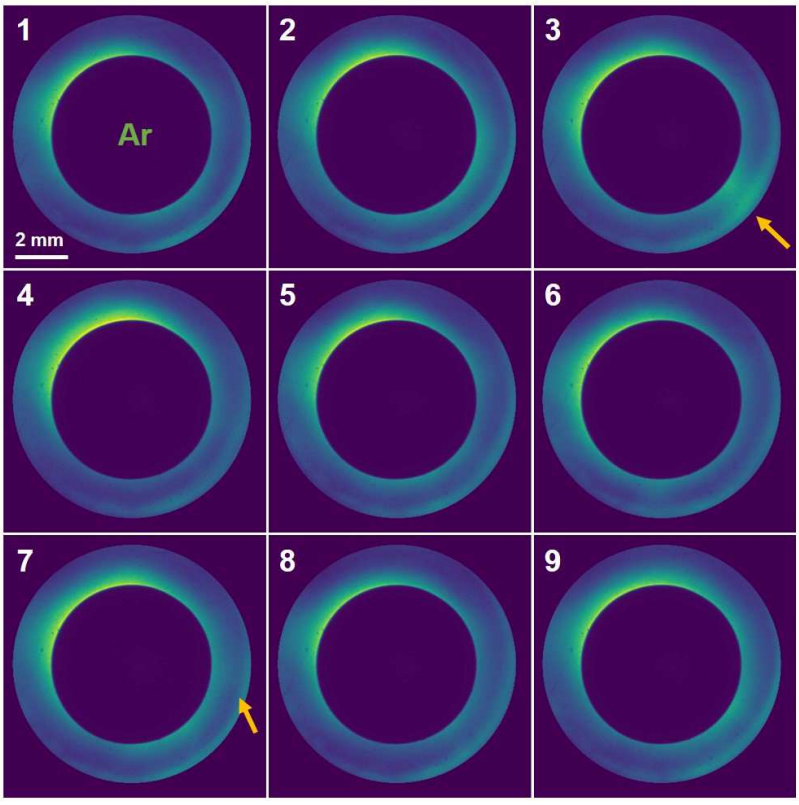

Figure 8

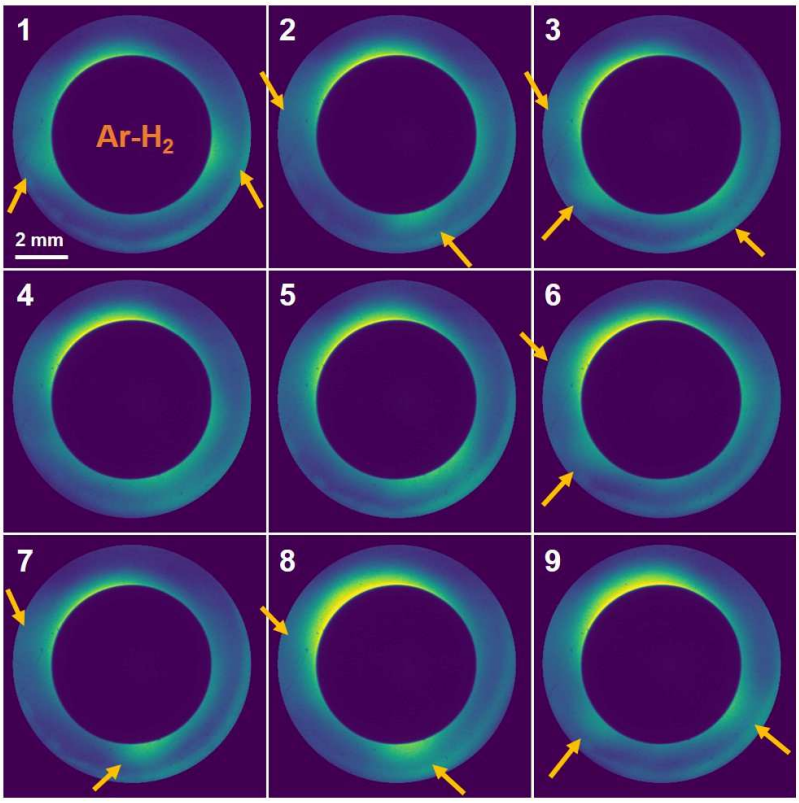

Figure 9

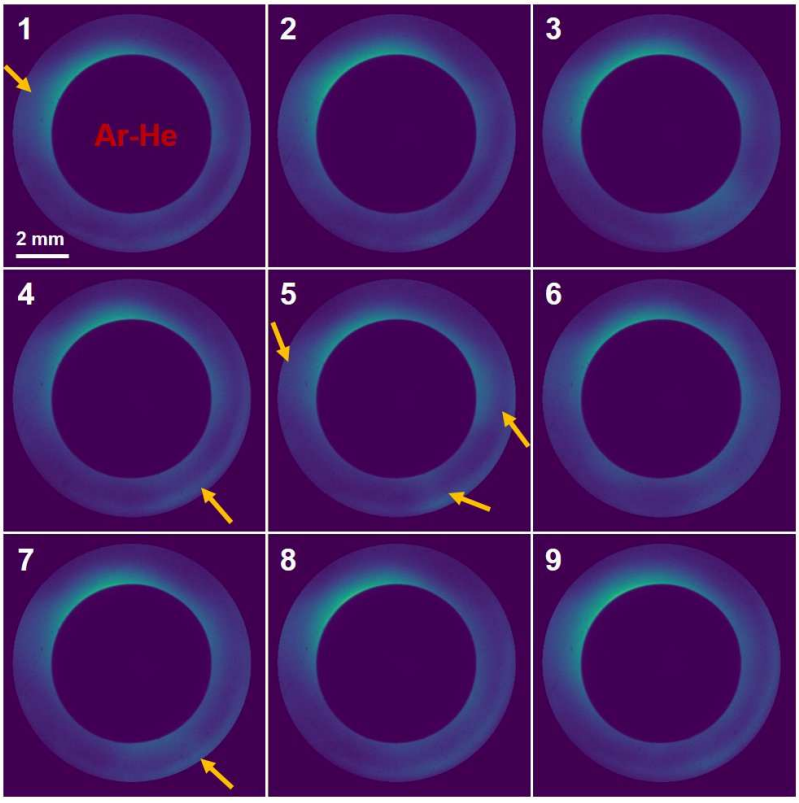

Figure 10

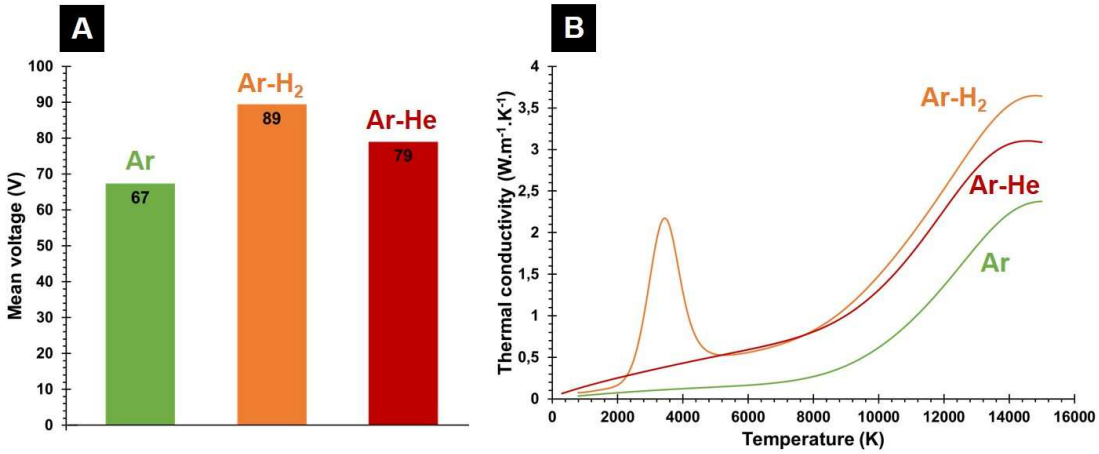

Figure 11

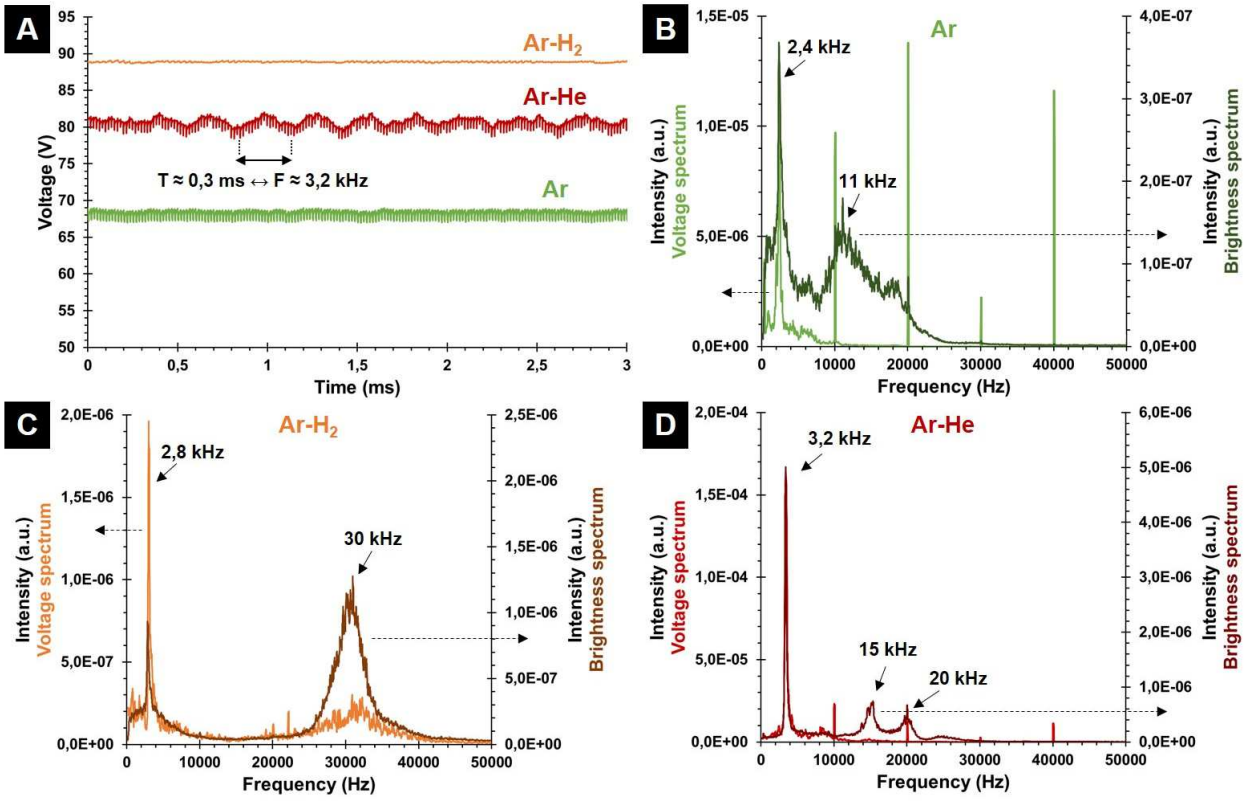

Figure 12

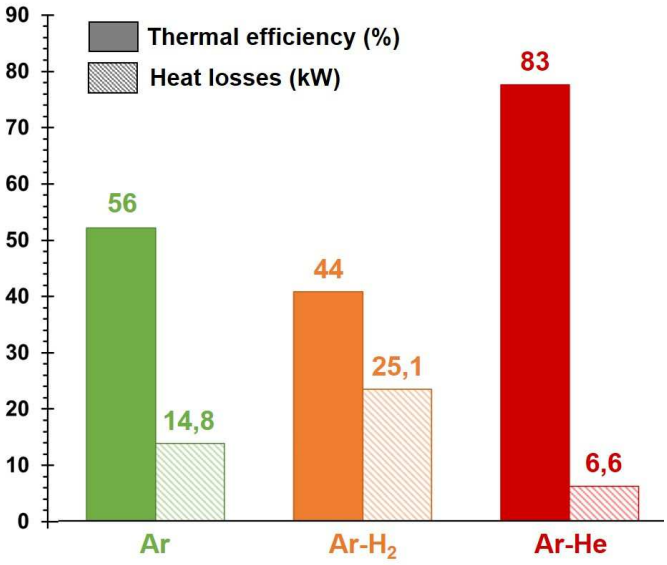

Figure 13

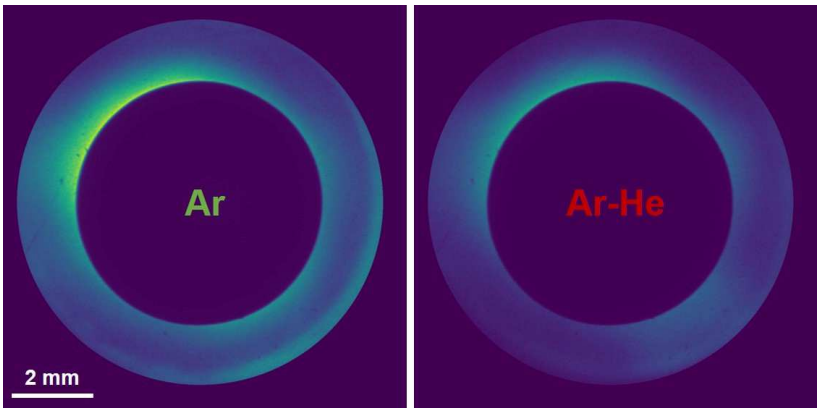

Figure 14

Supplementary material

Three videos in .avi are submitted with this article:

- Ar_500_A.avi: succession of 100 images for pure argon plasma at 500 A. Frame rate: 120 fps, exposure time: 60 ns.
- Ar-H2_500_A.avi: succession of 100 images for argon-hydrogen mixture at 500 A. Frame rate: 120 fps, exposure time: 60 ns.
- Ar-He_500_A.avi: succession of 100 images for argon-helium mixture at 500 A. Frame rate: 120 fps, exposure time: 60 ns.